Observed Aerosol and Liquid Water Path Relationships in Marine Stratocumulus

Xue Zheng[1], Bruce Albrecht[1], Patrick Minnis[2], Kirk Ayers[2], and Haf Jonson[3]

[1]Division of Meteorology and Physical Oceanography, Rosenstiel School of Marine and Atmospheric Science, University of Miami, Miami, FL, USA.

[2]NASA Langley Research Center Hampton, VA, USA.

[3]Naval Postgraduate School, Monterey, CA, USA.

The stratocumulus-topped marine boundary layer (BL), aerosol, and cloud properties observed on research flights made off the coast of northern Chile in the Southeastern Pacific (20°S, 72°W) during the VAMOS Ocean-Cloud-Atmosphere-Land Study-Regional Experiment (VOCALS-REx) were used to examine the variation of liquid water path (LWP) and cloud condensation nuclei (CCN). Ten flights were made under similar meteorological conditions where the BL structure was well-mixed, clouds were solid, and the conditions at the surface and at the top of the BL were similar. A strong positive correlation between the LWP, which varied from 15 to 73 gm^{-2}, and the BL CCN, which ranged from 190 to 565 cm^{-3}, was observed. Analysis of the two highest and the two lowest CCN concentration cases confirms that the differences in the thermodynamic jumps at the top of the BL and the turbulent fluxes at the surface cannot explain the observed differences in the LWP. Cloud properties from satellite retrievals combined with a back trajectories analysis demonstrated that the LWP differences observed at the time of the aircraft flights are also prevalent during the night-time hours prior to the aircraft observations. These results provide evidence for CCN and LWP relationships that are not fully explained by current hypotheses from numerical modeling.

1. Introduction

Anthropogenic aerosol particles are considered to modify marine stratocumulus cloud (Sc) properties by changing the cloud droplet size distribution [*Twomey*, 1977], and by suppressing drizzle processes, which could increase cloud amount, lifetime, and liquid water path (LWP) [*Albrecht*, 1989]. Although the first indirect effect has been established [e.g. *Lu and Seinfeld*, 2005; *Coakley and Walsh*, 2002 et al], the second indirect effect has controversial aspects and caveats that are revealed by numerical simulations [e.g. *Lu and Seinfeld*, 2005; *Hill and Feingold*, 2009] and satellite-based observations [*Coakley and Walsh*, 2002; *Brioude et al*., 2009].

Large-eddy simulations indicate that the introduction of aerosols can reduce cloud droplet size and inhibit cloud droplet sedimentation [*Ackerman*, 2004; *Bretherton*, 2007]. Thus, in this case, the enhanced evaporation and entrainment at the cloud top reduces LWP by 10% in Hill and Feingold (2009)'s simulations.. Wood [2007] used a mixed layer model to show that entrainment was enhanced in polluted clouds with high cloud bases resulting in a thinning of the cloud that was more significant than drizzle reduction in LWP during the first 24 hours of simulations. Satellite-based observations [*Christensen et al*, 2009] indicate that the cloud water content of polluted coastal marine stratus decrease from morning to afternoon at a slower rate than an unpolluted case.

There are two main challenges for observations [*Stevens and Feingold*, 2009]. First, satellite observations of aerosols are limited in cloudy regions. Further, in some cases it is difficult to use satellite observations to distinguish between cloud droplets and aerosols [*Koren et al,* 2007]. Second, for both satellite and in situ measurements, meteorological factors also

control the variation of cloud water content [*Stevens and Feingold*, 2009]. This study uses in-situ aircraft and remote satellite observations to investigate the relationship between cloud LWP and cloud condensation nuclei (CCN) concentration in Sc under relatively constant meteorological conditions.

2. Data and methods

Observations for this study were made using the CIRPAS Twin Otter aircraft on 18 flights over the subtropical southeastern Pacific at a fixed location (20°S, 72°W), designated as Point Alpha, during the VOCALS-REx from October 15 to November 15 2008. Instruments on the aircraft measured standard meteorological variables, turbulence, aerosol, cloud, and precipitation (Table1).

In this study, the objective criteria applied to select these 10 cases consisted of inversion heights between 1000 and 1300 m, potential temperature increased across the capping inversion ranging from 12-17°C, and total water content decreased across the inversion ranging from 6 to 8 g m^{-3}. The drizzle water contents from the Cloud Imaging Probe (CIP) on the 10 days were less than 10^{-3} g m^{-3}.Based on this analysis, the clouds occurring during these selected 10 days are assumed to exist in relatively similar meteorological conditions. Therefore, the influences of meteorological factors (including coastal effects) are assumed to be minimal. The majority (7) of the ten flights were made around 0900 Local Time (LT) (1200 UTC), while the others were conducted from around 1200 to 1300 LT.

The thermodynamic structures for these flights are shown in Figure 1 using a height scale normalized by the inversion height. These structures show well-mixed BL capped by sharp

58 inversions and similar BL thermodynamics for all the cases selected. The cloud thicknesses
59 and liquid water contents, however, for these cases vary substantially among the 10 cases.

60 For each flight day, all CCN measurements (at a super-saturation of 0.2%) below cloud base
61 and within 50 km of Point Alpha are averaged to give mean CCN concentrations. The sub-
62 cloud and above-inversion PCASP accumulation mode aerosol concentrations (PCASP
63 concentrations hereafter) in the sub-cloud layer and cloud droplet concentrations (Nc) in the
64 cloud layer are calculated in a similar way. The sounding of liquid water content (LWC) from
65 the Gerber probe is integrated to estimate LWP. The LWC from the soundings and the
66 horizontal leg averages at different levels have mean difference for all flights of 0.03±0.04
67 gm^{-3}, indicating that the LWC from soundings are representative of the larger-scale cloud area.
68 Vertical velocity observations (at 40 Hz) are used to calculate the vertical velocity variance
69 along the horizontal 10-minute legs at different levels. To further analyze the history of the
70 air masses sampled by the aircraft, we use the Hybrid Single Particle Lagrangian Integrated
71 Trajectory Model (HYSPLIT) model [*Draxler and Rolph*, 2003] driven with the NCEP
72 Global Data Assimilation System (GDAS) data to calculate the backward and forward
73 trajectories starting at Point Alpha and the 500-m level for 36 hours forward and backwards.
74 In addition, radiances from the Tenth Geostationary Operational Environmental Satellite
75 (GOES-10) were used to retrieve cloud properties using the methods of Minnis et al.
76 [2010a,b] for areas in the vicinity of the aircraft measurements and at times prior to and after
77 the measurements along the HYSPLIT trajectories.

3. Results

78 The CCN concentrations in the sub-cloud layer varied from 190 to 565 cm^{-3} among the 10
79 flights and were positively correlated with Nc, which ranged from 188 to 392 cm^{-3}. The LWPs
80 in these relatively thin clouds ranged from 15 to 73 gm^{-2} and are positively correlated with the
81 aerosol and Nc (Figure 2). The LWP estimated from the GOES analyses are also shown in
82 this figure. The average difference between the aircraft and satellite (50 km) LWP is -4.9 ±
83 13 gm^{-2} These results further support the idea that the sounding estimates of the LWP are
84 representative of a larger area as viewed by the satellite.

85 The positive correlation between the CCN concentrations and Nc are shown in Fig. 3 where
86 the probe concentrations are sorted from lowest to highest CCN concentrations. The
87 correlation between the CCN (and PCASP), and Nc is evident, although the deviation
88 between the CCN and Nc increases with increasing CCN (and PCASP) concentrations. The
89 PCASP concentrations above the inversion are lowest when the Nc are high and indicate no
90 major influence of the above-inversion aerosols on the BL aerosol conditions.

91 Backward trajectories for 9 of the 10 flights indicate a flow from the southeast of Point Alpha
92 from points close to the coast of Chile 36 hours earlier. During the 36 hour periods, 6 of the
93 air masses moved less than 500 km and remained over water, while the air masses for the
94 other 2 cases (Oct16 and 18) moved about 900 km from the south. The SST isotherms in this
95 area are oriented southeast to northwest, and since the synoptic patterns for the cases are
96 similar, advective effects did not vary substantially from case to case as indicated by the
97 similar trajectories on all but one case. The October 27 case indicates a major difference from
98 the others in that air began its 36-h journey near the southern coast of Peru. Although there
99 are uncertainties in these back trajectories due to errors in the GDAS, the errors should be
100 smallest in the early history of the trajectories.

To further investigate BL, aerosol, and cloud characteristics for the cases with high and low CCN concentrations, we averaged two cases (October 18 and 19) with the highest CCN (HC) and the two cases (October 27 and November 9) with the lowest CCN (LC). Characteristics of the BL, clouds, and aerosols for the HC and LC cases are given in Table 2. The HC PCASP concentration is about double that for the LC cases, which is consistent with the CCN values. The higher CCN concentrations for the HC cases are associated with Nc of 376 cm^{-3}, which are 153 cm^{-3} higher than that in the LC case. Both the mean in-situ LWP and the mean GOES LWP within a 20-km radius circle around Point Alpha are higher for the HC (65 $gm^{-2}$and 75 gm^{-2}) cases compared to those for the LC (18gm^{-2} and 36 gm^{-2}) cases. The LWP difference between HC and LC is significant and larger than the data uncertainty. The SST in the HC cases is 1.9°C lower than that for LC. The lower SSTs and surface wind speeds for the HC case are also associated with a surface virtual temperature flux ($F_{\theta v}$) that is 5.3 Wm^{-2} lower, and a water vapor flux (F_{qv}) that is 14.2 Wm^{-2} lower as well. The potential temperature jumps across the inversion are 15.8 K and 13.5 K for the HC and LC, respectively, and the corresponding total water content jumps are 7.3 and 6.5 g m^{-3}. The average HC cloud top is 138 m lower than its LC counterpart, while the HC cloud base is 240 m lower than that for the LC cases. The ratio of the observed LWP to the adiabatic LWP is about 0.83 compared with 0.56 for the LC data. Thus for the HC case the larger LWP is due to a cloud that is both thicker and closer to adiabatic than the LC cases.

Compared with the LC results, the HC cases have stronger and lower inversions, which are consistent with either stronger large-scale subsidence or weaker entrainment rates, if differences in the large-scale advection of the inversion are minimal. Using the eddy fluxes of total water at cloud top, the estimated entrainment rates $w_e = -(\overline{w'(q' + \ell')})/(\Delta q_t)$ are 1.0 and

124 1.8 mm/s respectively (1.2 to 1.5 mm/s for cloud averaged fluxes in this calculation. Further,
125 for a well mixed BL with negligible horizontal moisture advection, a local steady state would
126 give a total water flux at the inversion equal to the surface moisture flux giving entrainment
127 rates of 1.7 and 2.8 mm/s for the HC and LC cases respectively, which would be decreased by
128 a factor of 2 for dry advection of 0.5 -1.0 g/kg day^{-1}. Although there is substantially
129 uncertainty in these estimates of entrainment, they suggest that the entrainment rates in the
130 HC case are lower than those in the LC case (consistent with the lower HC inversion height),
131 although the w variance in the cloud layer (Table 2) is 0.26 m^{2}s^{-2} for the HC case compared
132 with 0.16 m^{2}s^{-2} in LC case.

133 To explore the time history of the observed differences in the LWP for the HC and LC cases,
134 the cloud properties along the back and forward trajectories from the GOES satellite retrievals
135 are also considered. Figure 4 shows the time evolution of LWP and cloud droplet effective
136 radius (R_e) for the HC and LC cases from 9 hours before to 3 hours after the flights each day.
137 On most of the flight days, one of the soundings was obtained around 1200 UTC, so the flight
138 time is set at 1145 UTC when the satellite data are available. In Figure 4, the flight time is
139 marked as t=0 hr, and the closed markers on the left side and right side of panel represent the
140 6-hour averaged values around 00 LT one day before and after the flight. The LWP from the
141 satellite retrievals decreased sharply after sunrise in all four cases. During the night, however,
142 the HC cases had much a much larger LWP than the LC cases. After sunrise, LWP in the HC
143 cases decreased, but remained larger than those in the LC cases. The relatively sharp drops in
144 LWP after sunrise, especially for the greater of the HC cases are due to the change in the
145 satellite retrieval algorithms between day and night [*Minnis et al.*, 2010a]. Nevertheless, the
146 nighttime algorithm shows some skill in discriminating between optically thick and thin

147 clouds and areas with small or large droplets, especially for Sc [*Minnis et al.*, 2010b]. The
148 time series of R_e for those four cases indicates that the HC cases had lower R_e values than
149 those for the LC cases during the entire period. The Lagrangian analysis indicates that the
150 observed features among these cases as observed by the aircraft may have existed at least 9
151 hours prior to the observations, which implies that the different LWP values for the extreme
152 cases mainly resulted from cloud evolution rather than differences in external meteorological
153 influences.

4. Summary and Discussion

154 The BL, aerosol, and cloud properties observed on ten research flights made off the coast of
155 Northern Chile indicate a strong positive correlation between BL CCN concentrations and
156 cloud LWP associated with similar BL and synoptic conditions. A detailed study of the two
157 highest and the two lowest CCN concentration (HC and the LC cases) further confirms that
158 the differences in the thermodynamic jumps at the top of the BL and the turbulent fluxes at
159 the surface cannot explain the observed differences in the LWP. Satellite retrievals from
160 GOES 10 show that the LWP differences observed at the time of the aircraft flights are also
161 prevalent during the night-time hours prior to the aircraft observations made at approximately
162 0900 local time. The cases with low LWP and CCN concentrations are associated with clouds
163 that are thinner and a water content that is a smaller fraction of the adiabatic value than the
164 high CCN and LWP cases.

165 The positive correlation observed in this study are inconsistent with some of the conclusions
166 from previous modeling studies [e.g. *Ackerman*, 2004; *Bretherton*, 2007; *Wood*, 2007] and
167 satellite analyses [e.g. *Coakley et al*. 2002]. In our study, the ratio of LWP and adiabatic

LWP is much less than unity in some clouds, which implies that processes such as entrainment and drizzle could be forcing cloud liquid water contents to deviate from the adiabatic values. The treatment of non-adiabatic clouds may cause problems in mixed layer formulations [e.g. Woods, 2007]. This study used the data collected around the same time of day, which minimizes the influence of diurnal cycle. Although the variance of the vertical velocity in the cloud layer associated with the thicker cloud is greater than that of the thinner clouds, we were unable to show that the entrainment rates for the high CCN case are significantly larger than the low CCN cases.

These results provide new evidence for CCN and LWP relationships that are not fully explained by current hypotheses from numerical modeling. Although the strategy we used here of comparing cases where the meteorology and the BL structure are very similar, we cannot eliminate the possibility that the changes in CCN may be associated with small changes in the large-scale forcing that in turn may also affect the LWP. True cause and effect cannot be established. Thus this work may motivate further studies to better explain the factors that control LWP and the role that the second indirect effects may play in the evolution of clouds.

Acknowledgments:

We are grateful for the dedicated efforts of several individuals in making the observations from the CIRPAS Twin Otter during VAMOS-REx. Drs. Graham Feingold and Patrick Chuang provided key scientific input on the observing strategies employed and interpretation of the initial results. Shaunna Donaher, Dione Rossiter, and Virendra Ghate, provided critical support as airborne scientists. Dr. Djamal Khelif kindly provided the high temporal

189 resolution observations for estimating turbulence quantities. Pilots Mike Hubble and Chris
190 McGuire skillfully executed the flight plans and endured the long ferry of the Twin Otter
191 aircraft to Iquique Chile and back. This research was supported by ONR Grant # xxxxxxxxx.

References

192 Ackerman, A. S., Kirkpatrick, M. P., Stevens, D. E. & Toon, O. B. (2004), The impact of humidity
193 above stratiform clouds on indirect aerosol climate forcing. *Nature 432*, 1014-1017

194 Albrecht, B.A. (1989): Aerosol, cloud microphysics, and fractional cloudiness. *Science*, 245, 1227-1230

195 Bretherton, C. S., Blossery, P. N., and Uchida J. (2007), Cloud droplet sedimentation, entrainment
196 efficiency, and subtropical stratocumulus albedo. Geophys. *Res. Lett., 34*, L03813, doi:
197 10.1029/2006GL027648.

198 Brioude, J., et al. (2009), Effect of biomass burning on marine stratocumulus clouds off the California
199 coast. *Atmos. Chem. Phys.*, *9*, 8841-8856.

200 Christensen, M. W., Coakley, J.A., and Tahnk W.R.(2009), Morning-to-Afternoon Evolution of
201 Marine Stratus Polluted by Underlying Ships: Implications for the Relative Lifetimes of
202 Polluted and Unpolluted Clouds, *J. Atmos. Sci., 66*, 2097-2106

203 Coakley, J.A., and C.D. Walsh (2002), Limits to the Aerosol Indirect Radiative Effect Derived from
204 Observations of Ship Tracks. *J. Atmos. Sci., 59*, 668–680.

205 Draxler, R.R. and Rolph, G.D., (2003), HYSPLIT (HYbrid Single-Particle Lagrangian Integrated
206 Trajectory) Model access via NOAA ARL READY Website. NOAA Air Resources Laboratory,
207 Silver Spring, MD.

208 Hill, A. A. and G. Feingold (2009), The Influence of Entrainment and Mixing Assumption on Aerosol–
209 Cloud Interactions in Marine Stratocumulus. *J. Atmos. Sci., 66*, 1450-1464

210 Koren, I., Remer, L. A., Kaufman, Y. J., Rudch, Y. and Martins, J. V. (2007), On the twilight zone
211 between clouds and aerosols. Geophys. *Res. Lett., 34*, L08805, doi:10.1029/2007GL029253

212 Lu, M.-L., and Seinfeld, J. H. (2005), Study of the aerosol indirect effect by large-eddy simulation of
213 marine stratocumulus. *J. Atmos. Sci., 62*, 3909-3932

214 Minnis, P., et al. (2010a), CERES Edition-2 cloud property retrievals using TRMM VIRS and Terra and
215 Aqua MODIS data, Part I: Algorithms, Submitted to *IEEE Trans. Geosci. Remote Sens.*

216 Minnis, P., et al. (2010b), CERES Edition-2 cloud property retrievals using TRMM VIRS and Terra and
217 Aqua MODIS data, Part II: Examples of average results and comparisons with other data, Submitted
218 to *IEEE Trans. Geosci. Remote Sens.*

219 Stevens, B. & Feingold, G. (2009), Untangling aerosol effects on clouds and precipitation in a buffered
220 system, *Nature, 461,* doi: 10.1038/nature08281

221 Twomey, S. (1977), Influence of pollution on shortwave albedo of clouds, *J.Atmos. Sci. 34*, 1149-1152

222 Wood, R. (2007), Cancellation of Aerosol Indirect Effects in Marine Stratocumulus through Cloud
223 Thinning. *J. Atmos. Sci., 64*, 2657-2669

Table 1 Instrumentations of Aerosol, Clouds and Precipitation Probes

Instrument	**Observations**	**Variables**
Gerber Probe	Liquid water	LWC
Cloud Imaging Probe (CIP)	Drizzle droplet size range: 25-1500 μm	Drizzle water content
CCN Spectrometer	CCN at 0.2% super-saturation	CCN
Passive Cavity Aerosol Spectrometer Probe	Aerosol size range: 0.1-2 μm	Accumulation mode aerosol concentration
Cloud, Aerosol and Precipitation	Cloud droplet size range: 2.07-40. μm	Cloud droplet concentration

Table 2 Cloud, Aerosol, and BL characteristics averaged for the two cases with the highest CCN and the two cases with the lowest CCN.

	HIGH CCN	LOW CCN	DIFF
PCASP (cm-3)	613	367	246
CCN (cm-3)	543	245	298
Nc (cm-3)	376	223	153
LWP (gm-2)	65	18	47
LWP-SAT (gm-2)	75	36	39
LWP/LWP-adia	0.79	0.61	0.18

SST (oC)	16.7	18.5	-1.8
$F_{\theta v}$ (Wm^{-2})	8.8	14.1	-5.3
F_q (Wm^{-2})	30.4	44.6	-14.2
$\overline{w'w'}$ (m^2s^{-2})	0.26	0.16	0.10
CLD TOP (m)	1050	1188	-138
CLD Base (m)	750	990	-240
$\Delta\theta$ (K)	15.8	13.5	-2.3
$-\Delta(q+\ell)$ (gm^{-3})	7.3	6.5	0.8
$\Delta\theta e$ (K)	4.1	4.6	-0.5

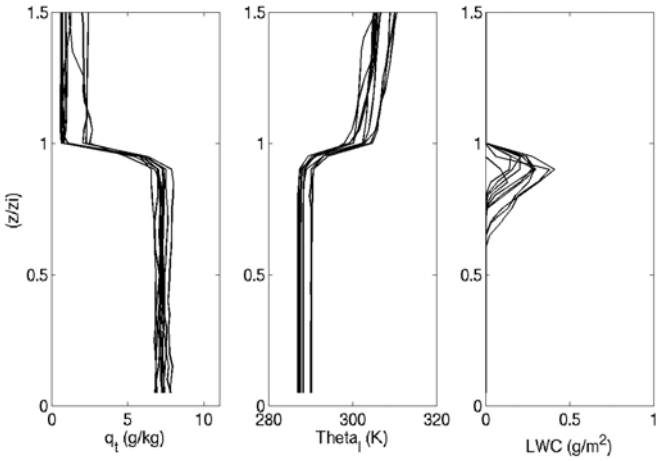

Figure 1. Vertical profiles of potential temperature, mixing ratio, and liquid water content for the ten cases in the study (Oct. 16, Oct. 18, Oct.19, Oct. 21, Oct. 22, Oct. 26, Oct. 27, Nov. 9, Nov. 10, Nov. 12, 2008)

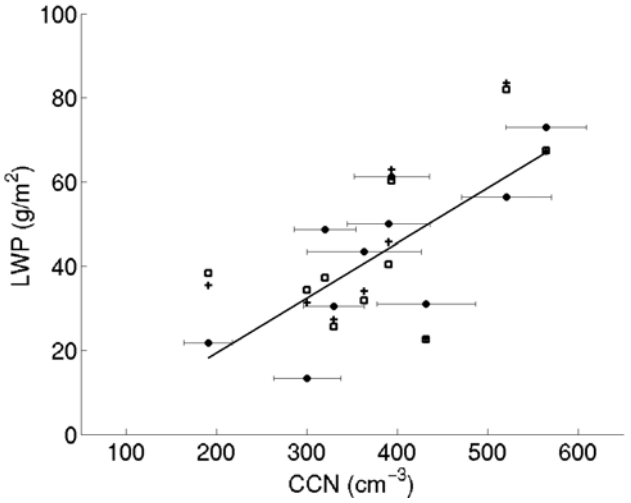

Figure 2. LWP as a function of sub-cloud CCN concentrations for selected 10 flights. Solid symbols are from aircraft profiles. The error bars through these symbols indicate the standard deviation of CCN. Cross and open symbols are averages from GOES retrievals within radii of 50 and 20 km, respectively. Line is a best fit to the aircraft LWP estimates.

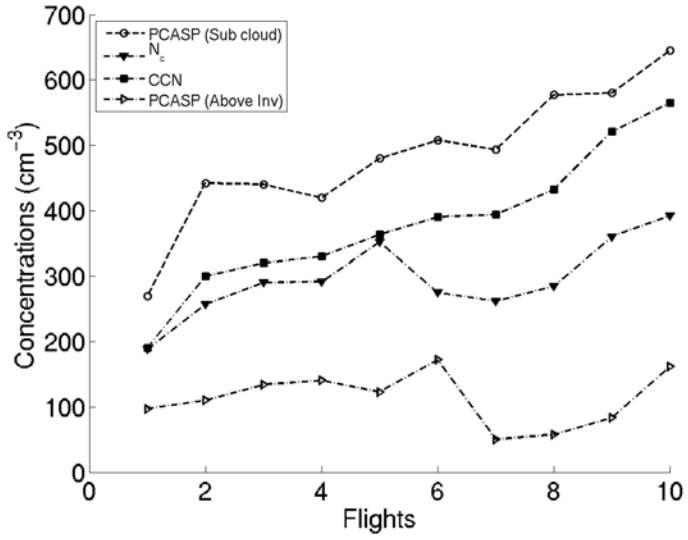

Figure 3 Sub-cloud layer CCN, PCASP and Nc for 10 cases sorted by increasing CCN from flight 1 to 10. Above-inversion PCASPs are also shown for comparison.

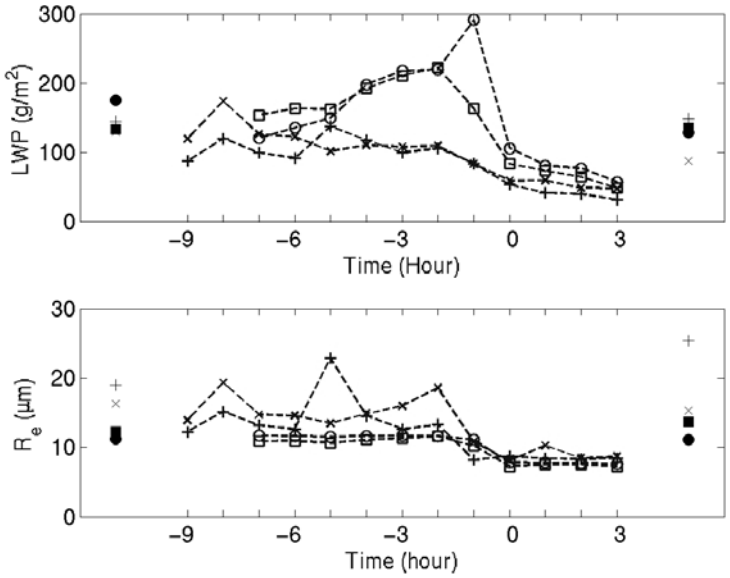

Figure 4. Time evolution of GOES-derived LWP and R_e for the two lowest (cross symbols) and the two highest (open symbols) CCN concentrations from 9 hours prior to the flight (marked as t=-9hr) to 3 hours after flight time (t=3hr). Solid dots at left and right sides of the lines are 6-hour averaged values during midnight one day before and one later.